The agreement obtained with Gurevich indicates that the simplification of the Boltzmann equation obtained by replacing $\mathbf{p}$ by $\mathbf{p}_{av}$ is a valid approximation for large magnetic field and may be of value in other contexts. It may be noted that the physical geometry of the crystal was essentially summed out of the problem by the operation of averaging $\mathbf{C}$ over the sample cross section. This technique may be used to treat cases of finite sample geometry with spherical energy surfaces if the averaging can be carried out over the cross section of the crystal. In addition the ellipsoidal-energy-surface case may be treated in this manner if the crystal boundaries map into a reasonable geometry under the Ham-Mattis transformation.

PHYSICAL REVIEW VOLUME 175, NUMBER 3 15 NOVEMBER 1968

# Dynamic Susceptibility of Magnetic Ions in Metals

YUNG-LI WANG* AND D. J. SCALAPINO†
*Physics Department, University of Pennsylvania, Philadelphia, Pennsylvania 19104*
(Received 31 May 1968)

We consider a magnetic dilute alloy system. The interaction between the localized magnetic moment and the conduction electrons is described by an *s-d* exchange Hamiltonian. The transverse susceptibility of the impurity spin is calculated in a Green's-function formalism. By employing the Wick and linked cluster theorems for spin systems developed by Wang and Callen, we have been able to analyze the Green's function diagrammatically. In the high-field low-temperature region ($\mu H \gg kT$) a partial summation of the main diagrams and lock diagrams gives, in addition to diagrams with self-energy structure, a set of diagrams with terminal parts. We have calculated the self-energy and the terminal function to the third-order in $N(O)J$, where $N(O)$ is the density of states at the Fermi surface and $J$ is the exchange parameter. It is shown that there is a $\ln H$ $g$ shift in the resonance frequency, and an $H \ln H$ correction to the analogous Korringa linewidth (which is linear in $H$). The magnetization is also calculated and is consistent with the earlier perturbation calculation.

## I. INTRODUCTION

GREAT interest has focused on the physics of dilute alloys containing magnetic impurities. Since Kondo's discovery of a $\ln T$ term which explained the low-temperature resistance minimum,[1] similar logarithmic terms have been found in perturbation theory for the magnetization.[2,3] Recently, Spencer and Doniach reported the calculation of a logarithmic shift of the electron-spin-resonance $g$ factor of the impurity[4] and Langreth *et al.*[5] analyzed in more detail the transmission paramagnetic resonance. Here we report a related perturbation theory calculation of the dynamic susceptibility of the impurity spin for the high-field low-temperature region $\mu H \gg kT$. We find in addition to a $\ln H$ shift of the $g$ value, that $\ln H$ terms appear in the linewidth and amplitude of the dynamic susceptibility. Implicit in these calculations is the assumption that the relaxation rate of the conduction electrons is much faster than that of the impurity spin. In the absence of a conduction-electron spin-lattice coupling the conduction-electron spins follow the impurity adiabatically, and these exchange-induced effects vanish for equal $g$ values of the conduction-electron and impurity spin.

A zero-temperature theory of this same system has been given by Giovannini and Koide[6] using a diagrammatic method derived from multiple contraction of spin operators. They considered only one class of second-order self-energy diagrams and did not obtain any of the logarithmic corrections. Spencer and Doniach,[4] using a drone-fermion representation for the impurity spin, summed an additional class of second-order self-energy diagrams and obtained a logarithmic shift in the $g$ value. However, they did not collect all terms in this order. Here we use a diagrammatic method based upon Schwinger's coupled-boson representation of the spin operators and the Wick-like theorem developed by Wang and Callen.[7,8] This allows the spin Green's function to be expressed in terms of a self-energy and a terminal function, each of which can then be calculated in perturbation theory when $\mu H \gg kT$. The consistency of this procedure is checked by evaluating the magnetization and comparing with the known perturbation-

* Supported at University of Pennsylvania by U. S. Office of Naval Research and at University of Pittsburgh by Air Force Office of Scientific Research. Present address: University of Pittsburgh, Pittsburgh, Pa.
† Supported by National Science Foundation.
[1] J. Kondo, Progr. Theoret. Phys. (Kyoto) 32, 37 (1964).
[2] K. Yosida and A. Okiji, Progr. Theoret. Phys. (Kyoto) 34, 505 (1965).
[3] D. J. Scalapino, Phys. Rev. Letters 16, 937 (1966).
[4] H. J. Spencer and S. Doniach, Phys. Rev. Letters 18, 994 (1967).
[5] D. C. Langreth, D. L. Cowan, and J. W. Wilkins, Solid State Commun. 6, 131 (1968).
[6] B. Giovannini and S. Koide, Progr. Theoret. Phys. (Kyoto) 34, 705 (1965).
[7] Y. L. Wang and H. Callen, Phys. Rev. 148, 433 (1966).
[8] Y. L. Wang, S. Shtrikman, and H. Callen, Phys. Rev. 148, 419 (1966).

theory results. In addition, for spin $\frac{1}{2}$, the sum rule

$$\langle S^+S^-\rangle+\langle S^-S^+\rangle=1 \tag{1.1}$$

is verified.

Before describing the detailed calculation, we summarize our results. The transverse dynamic susceptibility of an impurity of spin $S$ can be expressed in the form

$$\chi(\omega)=2S(1+\Lambda)/[\omega-\omega_0-2S\Sigma(\omega)]. \tag{1.2}$$

Here $\omega_0$ is the Zeeman energy $2\mu_BH$, $\Sigma$ is an irreducible self-energy part, and $\Lambda$ is the terminal function. Throughout the calculation, the bare $g$ values of the impurity and the conduction electrons have been set equal to 2. We have calculated the self-energy and the terminal function through third order in the exchange interaction. The results are that the peak of the imaginary part of $\chi(\omega)$ is shifted from the noninteracting value $\omega_0$ to

$$\omega_r=\omega_0\{1+\tfrac{1}{2}N(0)J+2[\tfrac{1}{2}N(0)J]^2\ln(\omega_0/D) +4[\tfrac{1}{2}N(0)J]^3\ln^2(\omega_0/D)\}. \tag{1.3}$$

This form suggests a geometric series which would sum to

$$\omega_r=\omega_0\left[1+\frac{\frac{1}{2}N(0)J}{1-N(0)J\ln(\omega_0/D)}\right]. \tag{1.4}$$

For antiferromagnetic coupling ($J<0$), this diverges when the magnetic field is reduced to a value determined by

$$g\mu_BH=D\exp[1/(N(0)J)], \tag{1.5}$$

and, in fact, becomes negative even before this. This is symptomatic of the failure of perturbation theory for fields such that $g\mu_BH/k_B$ is of the order of the Kondo temperature. The imaginary part of $\Sigma$ gives rise to a linewidth

$$\Gamma=2S\pi[\tfrac{1}{2}N(0)J]^2\omega_0[1+4\cdot\tfrac{1}{2}N(0)J\ln(\omega_0/D)], \tag{1.6}$$

which has the expected logarithmic contribution in third order. This departure of the linear dependence of the linewidth on the magnetic field is the main feature of the third-order calculation. For antiferromagnetic coupling the logarithmic term enhances the broadening, especially at lower fields. On the other hand, for ferromagnetic coupling, the linewidth is reduced. The terminal correction is given by

$$\Lambda=2[\tfrac{1}{2}N(0)J]^2\ln(\omega_0/D)+8[\tfrac{1}{2}N(0)J]^3\ln^2(\omega_0/D) \tag{1.7}$$

and corresponds to a reduction in the effective strength with which the impurity moment couples to the transverse magnetic field.

Using Eq. (1.2) for $\chi$ and the perturbation calculation of $\Sigma$ and $\Lambda$, the expectation values $\langle S^+S^-\rangle$ and $\langle S^-S^+\rangle$ are directly evaluated. From these, the expectation value of the magnetization is obtained:

$$2\mu_B\langle S^z\rangle=-2\mu_BS\{1+2[\tfrac{1}{2}N(0)J]^2\ln(\omega_0/D) +4[\tfrac{1}{2}N(0)J]^3\ln^2(\omega_0/D)\}. \tag{1.8}$$

This is in agreement with previous calculations,[9] and has the same divergent form as the expression for $\omega_r$ given in Eq. (1.3). Finally, for spin $\frac{1}{2}$, the sum rule Eq. (1.1) is checked. In both the magnetization and the sum rule, the presence of the terminal correction plays an essential role.

In Sec. II we briefly review the Wang-Callen formalism as it applies to the impurity problem. The susceptibility Green's function for the impurity is expressed in terms of self-energy and terminal functions. In Sec. III, calculations of the first- and second-order contributions to the self-energy and terminal functions at zero temperature are discussed and the results through third order are summarized. We conclude by formally extending these results to finite temperatures and note that the high-temperature form of the resulting expression for the static susceptibility agrees with the known perturbation-theory result.

## II. DIAGRAMMATIC REPRESENTATION OF THE IMPURITY SUSCEPTIBILITY

The dynamics of a single localized impurity of spin $S$ interacting with the conduction electrons in an external magnetic field $H$ will be described by a Hamiltonian

$$\mathcal{H}=\mathcal{H}_0+\mathcal{H}_1. \tag{2.1}$$

Here $\mathcal{H}_0$ is the sum of the electron quasiparticle energies

$$\epsilon_{k\sigma}=\epsilon_k+\mu_BH\sigma, \quad \sigma=\pm1, \tag{2.2}$$

and the Zeeman energy $\omega_0=2\mu_BH$ of the impurity spin

$$\mathcal{H}_0=\sum_{k\sigma}\epsilon_{k\sigma}C_{k\sigma}^\dagger C_{k\sigma}+\omega_0S^z. \tag{2.3}$$

For the purposes of this analysis, the coupling between the impurity and the conduction electrons will be written as a simple point-contact exchange interaction

$$\mathcal{H}_1=-\tfrac{1}{2}J\sum_{kk',\mu\nu}\mathbf{S}\cdot C_{k'\mu}^\dagger\boldsymbol{\sigma}_{\mu\nu}C_{k\nu}, \tag{2.4}$$

where $J$ is the exchange coupling and $(\sigma_{\mu\nu})_i$ are the Pauli matrices. The transverse susceptibility and the magnetization of the localized impurity can be determined from the spin Green's function:

$$G(t)=-i(0|PS^-(t)S^+(0)|0). \tag{2.5}$$

Here $|0)$ is the true ground state of the interacting system, the spin operators are in the Heisenberg representation, and $P$ is the Dyson time-ordering operator.

In the linked-diagram method of Wang and Callen, the spin operators are expressed in terms of Schwinger's coupled-boson operators:

$$\begin{aligned} S^+&=v^\dagger u,\\ S^-&=u^\dagger v,\\ S^z&=\tfrac{1}{2}(v^\dagger v-u^\dagger u)=-S+v^\dagger v. \end{aligned} \tag{2.6}$$

[9] B. Giovannini, R. Paulson, and R. Schrieffer, Phys. Letters 23, 517 (1966).

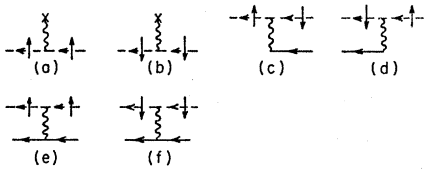


FIG. 1. The simple interaction vertices for a localized impurity of spin $S$ in the conduction electron sea. Solid lines represent $v$ propagators (spin propagators). Dashed lines represent electron propagators. The vertical wavy lines represent interactions. The diagrams (a) and (b) with a cross arise from the first term in the interaction Hamiltonian $\mathcal{H}_1$ of Eq. (2.8). Note that only $v$ propagators are drawn. The $u$ operators are taken care of implicitly by constructing the lock diagrams.

Here the last equality follows from the auxiliary constraint

$$v^\dagger v+u^\dagger u=2S, \tag{2.7}$$

which is equivalent to the condition $\mathbf{S}^2=S(S+1)$. The $u$'s and $v$'s are operators which satisfy boson commutation relations. Writing the Hamiltonian in terms of the $u$ and $v$ operators we have

$$\mathcal{H}_0=\sum_{k\sigma}\epsilon_{k\sigma}C_{k\sigma}^\dagger C_{k\sigma}+\omega_0 v^\dagger v-\omega_0 S,$$

$$\mathcal{H}_1=\tfrac{1}{2}J\sum_{kk'}[(-S+v^\dagger v)(C_{k\uparrow}^\dagger C_{k'\uparrow}-C_{k\downarrow}^\dagger C_{k'\downarrow}) \tag{2.8}$$
$$+v^\dagger u C_{k\downarrow}^\dagger C_{k'\uparrow}+vu^\dagger C_{k\uparrow}^\dagger C_{k'\downarrow}].$$

Invoking the usual "adiabatic turning-on theorem" for the effect of the perturbation $\mathcal{H}_1$ on the ground state and applying the linked diagram theorem for spin operators given in Ref. 7, the spin Green's function can be expressed in the form

$$G=-i\langle 0|Pv(t)v^\dagger(0)u^\dagger(t)u(0)\mathcal{S}(\infty)|0\rangle_{\text{connected}}. \tag{2.9}$$

Here $|0\rangle$ is the unperturbed ground state of $\mathcal{H}_0$, the time dependence of the $u(t)$ and $v(t)$ operators is determined by $\mathcal{H}_0$,

$$\begin{aligned} v^\dagger(t)&=e^{i\omega_0 t}v^\dagger(0),\\ v(t)&=e^{-i\omega_0 t}v(0),\\ u^\dagger(t)&=u^\dagger(0),\\ u(t)&=u(0), \end{aligned} \tag{2.10}$$

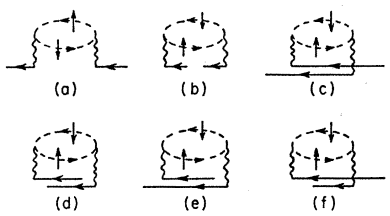


FIG. 2. Dependence of the diagrams on the weight associated with the ordering of the $v$ propagators. Diagrams (a) and (b) have weight factor $(2S)^2$ while diagrams (c) to (f) have weight factor $2S(2S-1)$.

and $\mathcal{S}(\infty)$ has the usual form

$$\mathcal{S}(\infty)=P\exp\left[-i\int_{-\infty}^{\infty}dt\,\mathcal{H}_1(t)\right]. \tag{2.11}$$

An expansion in powers of $\mathcal{H}_1$ gives various terms which can be represented by diagrams. As is usually the case, calculating with the final formalism is easier than explaining it. Since the details of the formalism are given in Ref. 7, we will simply illustrate some features of the method as it applies to the present problem. Let us focus on a second-order term in Eq. (2.9),

$$\sum_{kk'pp'}(-\tfrac{1}{2}J)^2(-i)^3\langle 0|Pv(t)v^\dagger(0)$$
$$\times u^\dagger(t)u(0)v(t_1)u^\dagger(t_1)v^\dagger(t_2)u(t_2)$$
$$\times C_{k\uparrow}^\dagger(t_1)C_{k'\downarrow}(t_1)C_{p\downarrow}^\dagger(t_2)C_{p'\uparrow}(t_2)|0\rangle. \tag{2.12}$$

This can be rewritten as

$$\sum_{kk'pp'}(-\tfrac{1}{2}J)^2(-i)^3\langle 0|Tv(t)v^\dagger(0)v(t_1)v^\dagger(t_2)|0\rangle$$
$$\times\langle 0|Tu^\dagger(t)u(0)u^\dagger(t_1)u(t_2)|0\rangle$$
$$\times\langle 0|TC_{k\uparrow}^\dagger(t_1)C_{k'\downarrow}(t_1)C_{p\downarrow}^\dagger(t_2)C_{p'\uparrow}(t_2)|0\rangle, \tag{2.13}$$

where we have replaced the Dyson's chronological ordering operators by Wick's chronological ordering operators. For Bose operators the two types of chronological operators are identical, while for Fermi operators this replacement is also justified since the Fermi operators always occur in pairs. Then it is obvious that to each product one can apply the conventional Wick's theorem which breaks the whole product into product of contracted pairs. However, as shown in Ref. 7 it is more convenient to treat the product of $u$ operators specially. Instead of applying Wick's theorem to the chronological product we evaluate it directly as a numerical "$u$ factor." This procedure is suggested by the fact that the $u$ operator carries no energy and that the $u$ operators are always introduced with the $v$ operators so that one can easily read the $u$ or $u^\dagger$ operators from the diagrams drawn for the $v$ operators. Applying Wick's theorem to the $v$ boson and the fermion parts of Eq. (2.13), it becomes

$$-\sum_{kp}(-\tfrac{1}{2}J)^2(-i)^3\langle 0|Tu^\dagger(t)u(0)u^\dagger(t_1)u(t_2)|0\rangle$$
$$\times(\langle 0|Tv(t)v^\dagger(t_2)|0\rangle\langle 0|Tv(t_1)v^\dagger(0)|0\rangle$$
$$+\langle 0|Tv(t)v^\dagger(0)|0\rangle\langle 0|Tv(t_1)v^\dagger(t_2)|0\rangle)$$
$$\times\langle 0|TC_{k\uparrow}(t_2)C_{k\uparrow}^\dagger(t_1)|0\rangle$$
$$\times\langle 0|TC_{p\downarrow}(t_1)C_{p\downarrow}^\dagger(t_2)|0\rangle. \tag{2.14}$$

Here the extra minus sign arises from the rearrangement of the Fermi operators.

This can be represented diagrammatically by imagining that the horizontal axis measures time increasing

from right to left. The $v$ propagator $\langle 0|Tv(t)v^\dagger(t_2)|0\rangle$ is represented by a solid line drawn from the point $t_2$ to the point $t$. The electron propagator $\langle 0|TC_{k\uparrow}(t_2)C_{k\uparrow}^\dagger(t_1)|0\rangle$ is similarly represented by a dashed line drawn from $t_1$ to $t_2$. Finally vertical wavy lines are used to represent interactions. The basic vertices associated with $\mathcal{H}_1$ are drawn in Fig. 1. Taking the first term in Eq. (2.14) and assuming $t>t_2>t_1>0$ we draw a diagram as shown in Fig. 2(a). Recalling that $|0\rangle$ has $2S$ $u$ particles and no $v$ particles, the $u$ factor for this time sequence reduces to $\langle 0|u^\dagger uu^\dagger u|0\rangle=(2S)^2$. On the other hand, when $t>t_1>t_2>0$ we obtain the diagram shown in Fig. 2(c), and the $u$ factor is $\langle 0|u^\dagger u^\dagger uu|0\rangle=2S(2S-1)$. It is immediately clear that whenever the two $v$ propagators overlap in time, as shown in Figs. 2(c)–2(f), the $u$ factor is $2S(2S-1)$ while the non overlapping Figs. 2(a) and 2(b) have $u$ factors $(2S)^2$.

The dependence of the diagrams on the weight associated with the ordering of the $v$ operators is an undesirable feature since it requires that the time integrations be done over the restricted time intervals whose number, in higher order of perturbation theory, increases catastrophically fast. This difficulty can be circumvented by introducing "main diagrams" in which

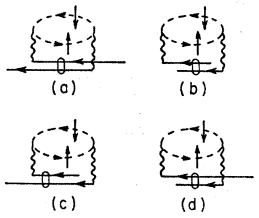


FIG. 3. Lock diagrams. To remove the dependence of the weight of the diagrams with different orderings of the $v$ propagators, a "main diagram" in which the time sequences of the propagator terminals are arbitrary is introduced with fixed weight $(2S)^2$. Then to compensate the incorrect weight given to the diagrams with ordering of $v$ propagators shown in Figs. 2(c) to 2(f), we introduce these lock diagrams with time sequences of the $v$ propagators restricted as shown and bearing a weight of $-2S$.

the time sequences of the propagator terminals are arbitrary and the $u$ factor is fixed at its maximum value. Then to compensate for the incorrect weight given to certain time orderings, an additional set of "lock diagrams" are introduced. These are represented by putting a small circle on overlapping $v$ propagator lines and are given the appropriate weight factor to correct for the error made by using a fixed weight factor in evaluating the main diagram. The time sequences of these lock diagrams are restricted. However, as shown in Ref. 7 the lock diagrams can be summed to obtain finally, an unrestricted set of diagrams. Here we illustrate this for the second-order diagrams. Figure 2(a) forms a main diagram, and the associated lock diagrams [Figs. 3(a)–3(d)] are obtained by putting a small circular "lock" on the overlapping $v$ propagators shown in Figs. 2(c)–2(f). Note that the time sequences of these lock diagrams are restricted as shown in each diagram.

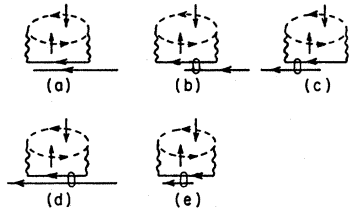


FIG. 4. A second type of contraction gives main diagram (a) and the associated lock diagrams (b) to (e). Diagram (a) is unlinked and has no contribution to the Green's function.

These diagrams are weighted by a factor $(-2S)$ so that when they are combined with the main diagram the correct "$u$ factor" weighting is restored. Similarly, the second type of contraction of the $v$ operators given in Eq. (2.14) reduces to the diagrams shown in Fig. 4. Since only linked diagrams contribute to $G$, the main diagram, Fig. 4(a) is discarded.

In order to remove the restrictions on the lock diagrams they are regrouped as shown in Fig. 5, where diagrams (a) and (b) are summed to diagram (A) and diagrams (c) and (d) are summed to diagram (B). In this form there are no restrictions on the time ordering of the vertices. The structure of the diagram (B) in Fig. 5 is characteristic of the spin problem. It has what we will call a terminal part. The other lock diagrams are combined in a similar way. The partial summation of the lock diagrams thus generates a new set of diagrams which has the form of the conventional diagrams aside from a new set of "terminal correction" diagrams.

We now proceed to a summary of the rules which allow us to evaluate the diagrammatic perturbation expansion of $iG$ in a systematic manner.

(1) With each spin line associate the function $iG_0=i2S(\omega-\omega_0+i\delta)^{-1}$. Here $\omega_0=2\mu_BH$ and $\delta$ is a positive infinitesimal.

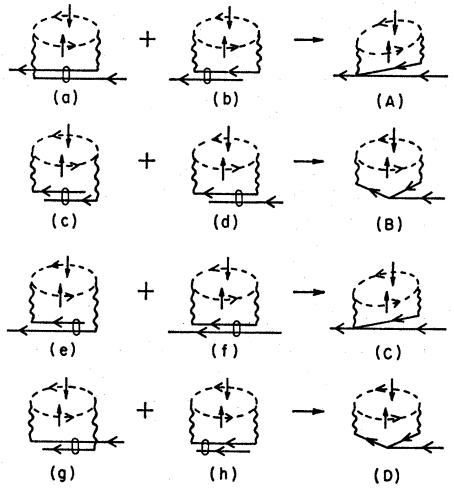


FIG. 5. A partial summation of lock diagrams removes the restriction of time sequences of the terminals of the $v$ propagators. In addition to diagrams with self-energy structure, terminal diagrams appear, as is characteristic of spin systems.

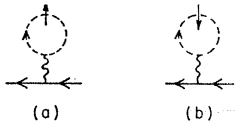


FIG. 6. The first-order diagrams.

(2) With each electron line associate the function $i(\omega-\epsilon_{k\sigma}+i\delta_\omega)^{-1}$, where $\epsilon_{k\sigma}$ is given by Eq. (2.2) and $\delta_\omega$ is an infinitesimal having the sign of $\omega$.

(3) With each transversal interaction line (i.e., spin-flip) associate the factor $\frac{1}{2}iJ$.

(4) With each longitudinal interaction line (i.e., non-spin-flip) associate the factor $(i/2S)(J/2)\sigma$, where $\sigma=1$ (or $-1$) for the interaction of local spin with an up (or down) spin electron.

(5) The external-fieldlike vertex [Figs. 1(a) and 1(b)] which arises from the first term in the interaction Hamiltonian is represented by a cross and a longitudinal interaction line. We associate with the cross a factor $-2S^2\sigma$, where $\sigma=\pm1$ as in rule 4.

(6) The grouping of the locked diagrams gives rise to a set of diagrams with "triple points" where three solid lines meet together. We associate with each triple point a factor $-2/(2S)^2$.

(7) Associate with each internal closed electron loop a factor $-1$.

(8) Sum over all electron momentum and integrate over all free-energy variables. In carrying out the summation over the electron momentum we will use a constant single-electron density of states over a symmetric energy band ($-D$ to $D$) about the Fermi energy.

As we mentioned earlier, the grouping of the lock diagrams not only enables us to reveal the self-energy portion of the propagator but also leads us to discover the set of terminal correction diagrams which have no analogue in the usual fermion or boson case. This set of terminal diagrams turns out to be particularly important in the evaluation of the magnetization and in satisfying the sum rule, Eq. (1.1), for the spin operators. Physically, the terminal corrections correspond to a renormalization of the effective transverse spin projection due to the interaction with the conduction electrons.

To sum the diagrams, we proceed as follows: First we construct a Green's function $\tilde{G}$ by summing the classes of diagrams which have the usual Dyson structure so that

$$\tilde{G}=G_0+G_0\Sigma\tilde{G}, \tag{2.15}$$

where $\Sigma$ is understood as the sum of the irreducible self-energy parts in the usual sense. We then note that for each of these diagrams there exist corresponding diagrams with terminal parts. Therefore, the total Green's function is obtained by collecting these additional diagrams

$$G=\tilde{G}+\Lambda\tilde{G}=(1+\Lambda)\tilde{G}. \tag{2.16}$$

Combining this with Eq. (2.15) we obtain

$$G=(1+\Lambda)/(G_0^{-1}-\Sigma), \tag{2.17}$$

where $\Lambda$ is the sum of all terminal parts. As we discussed, $\Lambda$ contributes to a renormalization of the response of the impurity moment to the transverse magnetic field. Having obtained the form for $G$ given by Eq. (2.16), the perturbation calculation reduces to evaluating $\Sigma$ and $\Lambda$ to a given order in $\mathcal{H}_1$.

## III. PERTURBATION CALCULATION OF $\Sigma$ AND $\Lambda$

The first-order self-energy diagram is shown in Fig. 6. According to the rules given in Sec. II, the contribution to the self-energy from this diagram is

$$\Sigma^{(1)}=-\tfrac{1}{2}JN(0)\frac{1}{2S}\sum_\sigma\int_{-D}^{D}d\epsilon_p\int\frac{d\omega}{2\pi i}\frac{1}{\omega-\epsilon_{p\sigma}+i\delta_\omega}$$
$$=-\tfrac{1}{2}N(0)J\frac{1}{2S}2\mu_BH. \tag{3.1}$$

There is no terminal correction so that in this order

$$G(\omega)=\frac{2S}{\omega-\omega_0[1+\frac{1}{2}N(0)J]+i\delta}, \tag{3.2}$$

and the resonance frequency is shifted from $\omega_0$ to $\omega_0[1+\frac{1}{2}N(0)J]$. In this order the matrix elements

$$\langle S^-S^+\rangle=-\int_0^D\frac{d\omega}{\pi}\mathrm{Im}G(\omega) \tag{3.3}$$

and

$$\langle S^+S^-\rangle=-\int_{-D}^0\frac{d\omega}{\pi}\mathrm{Im}G(\omega) \tag{3.4}$$

are simply evaluated and we find $\langle S^-S^+\rangle=2S$ and $\langle S^+S^-\rangle=0$. Therefore the magnetization is $-2\mu_BS$ and the sum rule Eq. (1.1) for spin $\frac{1}{2}$ is trivially satisfied.

Proceeding to the second order, one finds the four self-energy diagrams and the one terminal correction shown in Fig. 7. Again, using our rules, the contribution from the self-energy diagram [Fig. 7(a)] is

$$[\tfrac{1}{2}N(0)J]^2\int_{-D}^{D}d\epsilon_{p'}\int_{-D}^{D}d\epsilon_p\int\frac{d\omega'}{2\pi i}$$
$$\times\frac{1}{\omega'+\omega-\epsilon_{p\uparrow}+i\delta_{\omega'+\omega}}\frac{1}{\omega'-\epsilon_{p'\downarrow}+i\delta_{\omega'}}$$
$$=[\tfrac{1}{2}N(0)J]^2 4D\ln2-i\pi[\tfrac{1}{2}N(0)J]^2|\omega|. \tag{3.5}$$

Here, terms of order $[\frac{1}{2}N(0)J]^2\omega^2/D$ have been dropped. In the same way, the contributions from the remaining self-energy diagrams 7(b) to 7(g) are evaluated. Combining them, we find in the limit $\omega/D\ll1$ that

$$\Sigma^{(2)}=\frac{1}{2S}[\tfrac{1}{2}N(0)J]^2 2\omega_0\ln\frac{\omega_0}{D}-i[\tfrac{1}{2}N(0)J]^2\pi|\omega|. \tag{3.6}$$

The terminal diagram shown in Fig. 7(e) contributes

$$\Lambda^{(2)}=(-1)\frac{-2}{(2S)^2}[\tfrac{1}{2}iN(0)J]^2\int_{-D}^{D}d\epsilon_k\int_{-D}^{D}d\epsilon_q\int\frac{d\omega'}{2\pi}\times\int\frac{d\omega''}{2\pi}\frac{(2S)^2}{(\omega'-\omega_0+i\delta)^2}\frac{1}{\omega''-\epsilon_{q\downarrow}+i\delta_{\omega''}}\times\frac{1}{\omega'+\omega''-\epsilon_{k\uparrow}+i\delta_{\omega'+\omega''}}. \quad (3.7)$$

Carrying out the integration, $\Lambda^{(2)}$ reduces to

$$\Lambda^{(2)}=2[\tfrac{1}{2}N(0)J]^2\ln(\omega_0/D). \quad (3.8)$$

Therefore, the Green's function to second order is given as

$$G(\omega)=\frac{1+\Lambda^{(2)}}{G_0^{-1}-\Sigma^{(1)}-\Sigma^{(2)}}. \quad (3.9)$$

The dynamic susceptibility $\chi(\omega)$ is equal to $G(\omega+i0^+)$. Thus for positive values of $\omega$, the susceptibility to second order is given by

$$\chi(\omega)=\frac{2S(1+\Lambda^{(2)})}{\omega-\omega_r^{(2)}+i\Gamma^{(2)}}. \quad (3.10)$$

Here

$$\omega_r^{(2)}=\omega_0[1+\tfrac{1}{2}N(0)J+2[\tfrac{1}{2}N(0)J]^2\ln(\omega_0/D)], \quad (3.11)$$

$$\Gamma^{(2)}=2S[\tfrac{1}{2}N(0)J]^2\pi 2\mu_BH, \quad (3.12)$$

$$\Lambda^{(2)}=2[\tfrac{1}{2}N(0)J]^2\ln(\omega_0/D), \quad (3.13)$$

and $\Gamma^{(2)}$ has been evaluated at $\omega=\omega_r\cong 2\mu_BH$. The resonance frequency of the impurity spin is shifted in the second order by a log term in magnetic field. The logarithmic term in the $g$ shift is similar[10] to that reported by Spencer and Doniach.[4] In addition, we find that the amplitude of the susceptibility is modified. $\Gamma^{(2)}$ is the half-width and is linearly proportional to the applied magnetic field. This is just the analog of the Korringa broadening[11] at zero temperature, where $\omega_0$, the Zeeman energy, takes the place of $kT$. However, there is difference of the line broadening due to the $T_1$ process considered by Korringa and that due to the $T_2$ process calculated here. In case of $kT\gg g\mu_BH$, the thermal fluctuation washes out the anisotropy introduced by the Zeeman term in the Hamiltonian, and $T_2$ is equal to $T_1$ as expected. On the other hand, when $kT\ll g\mu_BH$ we find

$$1/T_2=2S\pi[\tfrac{1}{2}N(0)J]^2g\mu_BH,$$

compared with

$$1/T_1=4\pi[\tfrac{1}{2}N(0)J]^2g\mu_BH.$$

[10] If $\omega_0$ is replaced by $kT$ in the argument of the logarithm, this result differs by a factor of 2 from that reported by Spencer and Doniach but agrees with that obtained by Langreth, Cowan, and Wikins.

[11] J. Korringa, Physica **16**, 609 (1950).

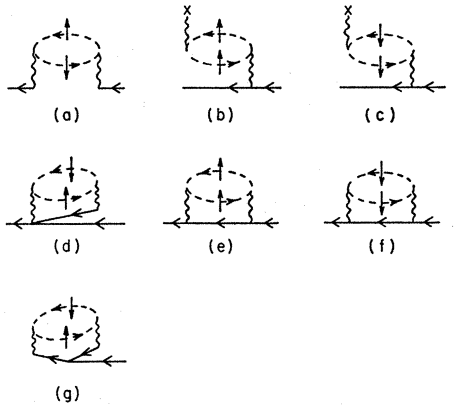


FIG. 7. Second-order self-energy diagrams and the terminal diagram.

In order to check the consistency of our second-order calculation we turn to an evaluation of the matrix elements $\langle S^+S^-\rangle$ and $\langle S^-S^+\rangle$. Inserting the spectral weight,

$$-\frac{1}{\pi}\mathrm{Im}G(\omega)=\frac{(2S)^2(1+\Lambda)[\tfrac{1}{2}N(0)J]^2|\omega|}{(\omega-\omega_r)^2+[\tfrac{1}{2}N(0)J]^4\pi^2(2S)^2\omega^2}, \quad (3.14)$$

into Eqs. (3.3) and (3.4) we obtain

$$\langle S^+S^-\rangle=-(2S)^2[\tfrac{1}{2}N(0)J]^2\ln(\omega_0/D), \quad (3.15)$$

$$\langle S^-S^+\rangle=2S+2S(2-2S)[\tfrac{1}{2}N(0)J]^2\ln(\omega_0/D). \quad (3.16)$$

Therefore,

$$\langle S^z\rangle=\tfrac{1}{2}(\langle S^+S^-\rangle-\langle S^-S^+\rangle)=-S\{1+2[\tfrac{1}{2}N(0)J]^2\ln(\omega_0/D)\}, \quad (3.17)$$

which is consistent with the static calculation by Giovannini, Paulson, and Schrieffer[9] for $S=\frac{1}{2}$. The sum rule for $S=\frac{1}{2}$,

$$\langle S^+S^-\rangle+\langle S^-S^+\rangle=1, \quad (3.18)$$

is also verified by adding Eq. (3.15) and Eq. (3.16). This provides a further check on the form of the calculated Green's function and the resultant susceptibility $\chi$. We note that both of these results can only be obtained by including the terminal vertex correction diagram which is unique to the spin problems.

There are a large number of third-order diagrams, but their evaluation is straightforward. Applying the rules given in the above section we have evaluated all the self-energy diagrams and the terminal vertex parts. Retaining only the most singular terms and evaluating $\Sigma$ at $\omega_r$ we obtain through third order the following resonance frequency and linewidth parameters:

$$\omega_r=\omega_0\{1+\tfrac{1}{2}N(0)J+2[\tfrac{1}{2}N(0)J]^2\times\ln(\omega_0/D)+4[\tfrac{1}{2}N(0)J]^3\ln^2(\omega_0/D)\}, \quad (3.19)$$

$$\Gamma=2S[\tfrac{1}{2}N(0)J]^2\pi\omega_0\{1+4[\tfrac{1}{2}N(0)J]\ln(\omega_0/D)\}. \quad (3.20)$$

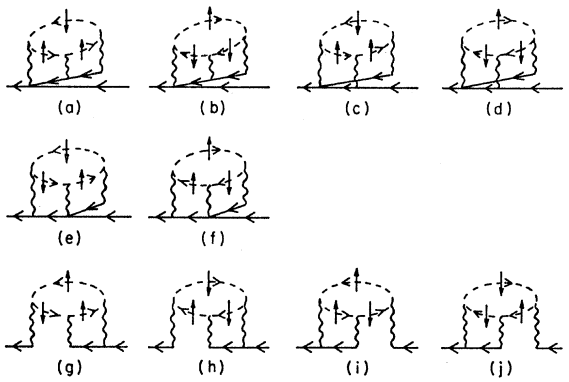


FIG. 8. Third-order self-energy diagrams which give the $\ln^2 H$ shift in the resonance frequency and an $H \ln H$ correction to the linear $H$ dependence in the linewidth.

The relevant diagrams are shown in Fig. 8. Where diagrams (a) to (f) give the $\ln^2(\omega_0/D)$ shift of resonance frequency and diagrams (g) to (j) give the $\omega_0 \ln(\omega_0/D)$ correction to the linewidth.

The magnetization can also be calculated, and to the third order of $N(0)J$ we find

$$\langle S^z\rangle = -S\{1+2[\tfrac{1}{2}N(0)J]^2 \ln(\omega_0/D) + 4[\tfrac{1}{2}N(0)J]^3 \ln^2(\omega_0/D)\}, \quad (3.21)$$

which is consistent with the earlier perturbation calculation.[9] The sum rule, Eq. (1.1), for spin $\frac{1}{2}$ is also satisfied in this order.

The most interesting feature in the third-order calculation is the appearance of the $\ln H$ term in the linewidth. The linear dependence of the second-order line broadening upon magnetic field is therefore modified. In the case of antiferromagnetic coupling where $J<0$ the linewidth is enhanced by the logarithmic term. On the other hand, for ferromagnetic coupling, the linewidth is reduced.

## IV. EXTENTION TO FINITE TEMPERATURE

The zero-temperature perturbation method which has been used to calculate $\chi(\omega)$ is suitable when $2\mu H$ is large compared with the Kondo energy $D\exp-[1/(N(0)J)]$. Using the Matsubara temperature ordered Green's functions, a similar analysis for spin $\frac{1}{2}$ can be carried out at finite temperature. However, the regrouping procedure for the half-overlapping diagrams is accurate only to order $\exp(-2\mu_B H/kT)$. This approach is therefore restricted to the low-temperature high-magnetic-field regime. However, it is interesting to note that if we formally replace $\omega_0$ by $kT$ in the argument of the logarithmic functions we obtained the high-temperature results to logarithmic accuracy. We briefly illustrate this, for $S=\frac{1}{2}$.

$$\chi^{-+}(\omega) = \frac{(1+\Lambda)\tanh(\beta\omega_r/2)}{\omega-\omega_r+i\Gamma} \quad (4.1)$$

with

$$\begin{aligned} \omega_r &= \omega_0\{1+\tfrac{1}{2}N(0)J+2[\tfrac{1}{2}N(0)J]^2 \ln(kT/D)\}, \\ \Lambda &= 2[\tfrac{1}{2}N(0)J]^2 \ln(kT/D), \\ \Gamma &\sim [\tfrac{1}{2}N(0)J]^2 \pi kT. \end{aligned} \quad (4.2)$$

The function $\tanh(\beta\omega_r/2)$ arises from the thermal average of $S^z$ in the effective field $\omega_r/(g\mu_B)$. The function exists of course even if $J=0$ and reduces to unity at $T=0$. For $\Gamma \ll kT$ we can approximate the imaginary part of $\chi^{-+}$ by a $\delta$ function. Therefore,

$$\langle S^z\rangle = \tfrac{1}{2} - \frac{1}{\pi}\int_{-\infty}^{\infty} d\omega \frac{1}{1-e^{-\beta\omega}} \mathrm{Im}\chi^{-+}(\omega) \quad (4.3)$$

$$= -\tfrac{1}{4}\beta\omega_r(1+\Lambda) \quad (4.4)$$

$$= \langle S^z\rangle_0\{1+\tfrac{1}{2}N(0)J+[N(0)J]^2 \ln(kT/D)\}, \quad (4.5)$$

where $\langle S^z\rangle_0 = -\frac{1}{4}\beta\omega_0$ is the expectation value of $S^z$ at high temperature when $J=0$. This result, Eq. (4.5), is consistent with that obtained by Giovannini, Paulson, and Schrieffer[9] and the calculation of Scalapino[3] using an Anderson model.

## ACKNOWLEDGMENT

We would like to thank Professor H. B. Callen for many helpful and stimulating discussions.